CEAS-GNC-2022-026

CEAS EuroGNC 2022
"Conference on Guidance, Navigation and Control"
3-5 May 2022 @ Technische Universität Berlin, Germany

Cooperative Platooning and Servicing for Spacecraft Formation Flying using Model Predictive Control

Pedro Pereira Master Student, NOVA School of Science and Technology, DEEC, 2829-516, Caparica, Portugal. Software Engineer, Volkswagen Digital Solutions, MAN Digital Hub, 1000-138, Lisbon, Portugal. pmp.pereira@campus.fct.unl.pt

Bruno Guerreiro Assistant Professor, NOVA School of Science and Technology, DEEC and CTS/Uninova, 2829-516, Caparica, Portugal. Senior Researcher, LARSYS, ISR-Lisbon, 1049-001, Lisbon, Portugal. bj.guerreiro@fct.unl.pt

Pedro Lourenço GNC Engineer, GMV, GNC Division, Space Segment and Robotics BU, 1990-392, Lisbon, Portugal. palourenco@gmv.com

ABSTRACT

This paper addresses two complementary problems of spacecraft formation flying, namely spacecraft platooning and on-orbit spacecraft servicing, using Model Predictive Control (MPC). With the proposed solutions, these space formation scenarios can be regarded as a cooperative system composed of several spacecraft with a common goal, which may have clear advantages relative to other approaches. For each application scenario, a different optimization problem and MPC design is presented, including relevant constraints to deal with physical limitations, visibility problems, and also to guarantee a collision-free trajectory from other spacecraft or obstacles. The proposed methods are validated with realistic simulation results, showing that all vehicles demonstrate reliable performance following a given trajectory or goal in a formation, while satisfying all the considered constraints.

Keywords: MPC; Spacecraft Formation Flying; Cooperative Control; Platooning; On-Orbit Servicing

1 Introduction

Space exploration has been a much discussed topic in recent years, due to the inherent curiosity of wanting to know more about how the Universe works, and possibly to take Human society outside of planet Earth. Within the immense complexity of planning and implementing a spacecraft for space navigation, some of the most important and difficult maneuvers to perform are the rendezvous and docking maneuvers [1], which make it possible to physically couple two spacecraft. These maneuvers are essential for example to transport goods or people from one spacecraft to another, for replenishment, assembly, maintenance, repair [2], and also for the collection of space debris [3–5] which threatens the preservation of active spacecraft orbiting the Earth. These maneuvers need not only to perform successfully all these tasks but also incorporate autonomy into the systems, relying as little as possible in external human aid.

Over the years, different methods were considered for these proximity operations, but due to the computational limitations in space [6, 7], there has been a focus on simpler and computationally lighter methods. Recently, with the development of more robust and capable embedded systems, more complex

controllers started being considered for space operations, and among them is Model Predictive Control (MPC). MPC was initially considered for industrial applications, to control oil refineries, power plants and chemical processes [8], but due to its performance while allowing constraint satisfaction, the MPC has been in recent years vastly studied for flight control, docking and rendezvous maneuvers [9–18]. One application is spacecraft formation flying [19–22], that consists in the cooperation of several spacecraft to achieve a specific objective, instead of sending a single, more expensive spacecraft. This topology allows to obtain a distributed model [23–25] between all the spacecraft, but sharing at the same time a common objective. In this case two different scenarios are proposed, that can be viewed as two different phases of flight formation.

The first proposed strategy in this work addresses a spacecraft platooning system [26], where several follower spacecraft converge to the leader spacecraft orbit and establish a constant relative position and velocity between each other. This is achieved using a Distributed Model Predictive Control (DMPC) strategy, where the system model consists of a coupled relative model between each spacecraft with a V-bar orbital station keeping trajectory. A spacecraft platooning system can have several uses, such as synchronization, position correction, spacecraft retention on a specific orbit and also for Earth observation, where a system of spacecraft can orbit around the Earth and retrieve soil or meteorological information to be later analyzed and compared.

The second proposed strategy in this work addresses an on-orbit spacecraft servicing system, where a group of spacecraft moves around an object in order to achieve a specific goal, for example, observation, repair, delivery or a synchronized docking. The spacecraft use the relative position between themselves and the object to move around and get to the desired positions, but also considering other spacecraft to avoid collisions. In addition to that, since observation can be one application for this scenario, it is included not only the relative translational dynamics but also the relative rotational dynamics, in order to allow the spacecraft to point to a specific coordinate in the object. As the motion equations are intrinsically nonlinear, a Nonlinear Model Predictive Control (NMPC) strategy is considered, with cooperative coupled constraints.

The contributions of this paper include an extension of the typical problem of on-orbit spacecraft servicing and spacecraft synchronization, resorting not only to an optimal controller like the MPC, but also incorporating the concept of cooperation and distribution between each spacecraft, which results in a more capable and efficient system overall. The spacecraft platooning system differs from other approaches by linking the relative models through the control action and the spacecraft servicing system presents a new cooperative solution. Methods that are validated through simulation results, showing reliable performance while satisfying all the considered constraints.

The remainder of this paper is structured as follows. Section 2 contains a brief background of spacecraft formation flying dynamics. Section 3 outlines the MPC design for the spacecraft platooning system, including the joint state-space model, the distributed optimal control problem and the constraints. Section 4 outlines the MPC design for the on-orbit spacecraft servicing system, including the coupled translational and rotational model, the nonlinear optimal control problem, the constraints and the attitude trajectory planning. Simulation results for the systems in Sections 3 and 4 are presented in Section 5. Conclusions and future work are discussed in Section 6.

2 Relative Motion Model of Spacecraft

This Section introduces the general notation and mathematical background for spacecraft formation flying starting with the coordinate reference frames used throughout the paper, moving on to the relative translational motion and finally the relative rotational motion for spacecraft.

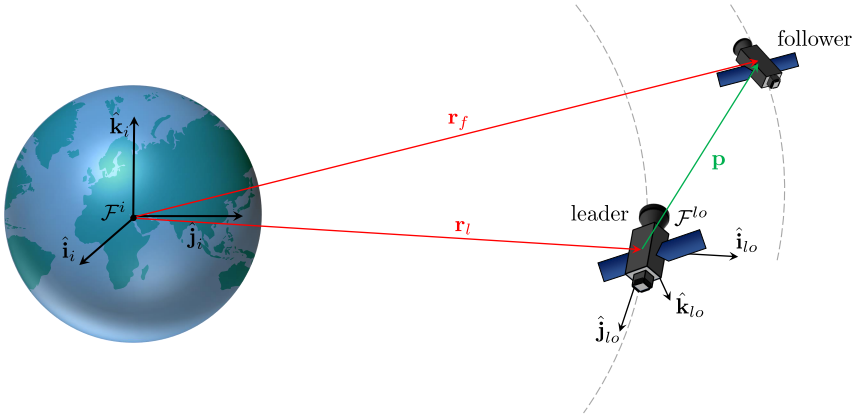

Fig. 1 Reference coordinate frames in a leader-follower formation

2.1 Coordinate Reference Frames

Earth Centered Inertial (ECI) Frame, denoted as $\mathcal{F}^i : \{O_i, \hat{\mathbf{i}}_i, \hat{\mathbf{j}}_i, \hat{\mathbf{k}}_i\}$, has its origin located in the center of the Earth. The $\hat{\mathbf{i}}_i$ axis is directed towards the vernal equinox, $\hat{\mathbf{k}}_i$ is directed along the rotation axis of the Earth towards the celestial North Pole and $\hat{\mathbf{j}}_i$ completes the right-handed orthogonal frame.

Spacecraft Orbit Reference Frame, denoted as $\mathcal{F}^{so} : \{O_s, \hat{\mathbf{i}}_{so}, \hat{\mathbf{j}}_{so}, \hat{\mathbf{k}}_{so}\}$, is a Local-Vertical-Local-Horizontal (LVLH) frame with its origin located in the center of mass of the spacecraft. The $\hat{\mathbf{i}}_{so}$ axis is directed along the radius vector ${}^i\mathbf{r}_s \in \mathbb{R}^3$ in the $\mathcal{F}^i$ frame, that goes from the center of the Earth to the spacecraft, $\hat{\mathbf{k}}_{so}$ is pointing in the orbit normal direction, parallel to the orbit momentum vector and $\hat{\mathbf{j}}_{so}$ completes the right-handed orthogonal frame. The basis vectors of $\mathcal{F}^{so}$ can be defined as

$$\hat{\mathbf{i}}_{so} = \frac{{}^i\mathbf{r}_s}{\|{}^i\mathbf{r}_s\|}, \quad \hat{\mathbf{j}}_{so} = \hat{\mathbf{k}}_{so} \times \hat{\mathbf{i}}_{so}, \quad \hat{\mathbf{k}}_{so} = \frac{\mathbf{h}}{\|\mathbf{h}\|} \tag{1}$$

where $\mathbf{h} = {}^i\mathbf{r}_s \times {}^i\dot{\mathbf{r}}_s$ is the angular momentum vector of the orbit and s denotes the spacecraft in question, e.g. $s = l$ for the leader and $s = f$ for the follower.

Spacecraft Body Reference Frame, denoted as $\mathcal{F}^{sb} : \{O_s, \hat{\mathbf{i}}_{sb}, \hat{\mathbf{j}}_{sb}, \hat{\mathbf{k}}_{sb}\}$, has its origin located in the center of mass of the spacecraft, with the basis vectors aligned with the principal body axes.

2.2 Relative Translational Motion

Consider a leader-follower spacecraft formation, where the position vector of the leader and the follower expressed in $\mathcal{F}^i$ are defined respectively as ${}^i\mathbf{r}_l$ and ${}^i\mathbf{r}_f$, as seen in Fig. 1.

Resorting to the Keplerian two-body problem, the orbital dynamics for both spacecraft can be expressed as

$${}^i\ddot{\mathbf{r}}_l = -\frac{\mu}{\|{}^i\mathbf{r}_l\|^3}{}^i\mathbf{r}_l, \quad {}^i\ddot{\mathbf{r}}_f = -\frac{\mu}{\|{}^i\mathbf{r}_f\|^3}{}^i\mathbf{r}_f + \frac{1}{m_f}{}^i\mathbf{f}_f \tag{2}$$

where ${}^i\mathbf{f}_f \in \mathbb{R}^3$ is the actuator forces of the follower in the $\mathcal{F}^i$ frame, m_f is the follower mass, and μ is the geocentric gravitational constant given by $\mu \approx Gm_\oplus$, where G is the universal gravitational constant and $m_\oplus$ is the Earth mass. Orbital perturbations are neglected.

The relative position vector between the leader and the follower can therefore be expressed in the orbital frame $\mathcal{F}^{lo}$ as

$$\mathbf{p} = \mathbf{R}_i^{lo}({}^i\mathbf{r}_f - {}^i\mathbf{r}_l) = \begin{bmatrix} x & y & z \end{bmatrix}^T \tag{3}$$

and the relative velocity as $\mathbf{v} = \dot{\mathbf{p}}$, where $\mathbf{R}_i^{lo} \in \mathcal{SO}(3)$ is the rotation matrix from $\mathcal{F}^i$ to the $\mathcal{F}^{lo}$ frame and $\mathcal{SO}(3)$ is the 3D rotation group defined as $\mathcal{SO}(3) = \{\mathbf{R} \in \mathbb{R}^{3\times3} : \quad \mathbf{R}^T\mathbf{R} = \mathbf{R}\mathbf{R}^T = \mathbf{I}_3, \quad \det(\mathbf{R}) = 1\}$ with $\mathbf{I}_3 \in \mathbb{R}^{3\times3}$ as the identity matrix.

From expressions (2) and (3), a nonlinear relative translational dynamics can be derived for circular orbits [27], given by

$$\dot{\mathbf{v}} = \mathbf{C}_t\mathbf{v} + \mathbf{D}_t\mathbf{p} + \mathbf{E}_t + \mathbf{F}_t \tag{4}$$

where

$$\mathbf{C}_t = -2n\begin{bmatrix}0 & -1 & 0\\ 1 & 0 & 0\\ 0 & 0 & 0\end{bmatrix}, \quad \mathbf{D}_t = -\begin{bmatrix}\frac{\mu}{\|{}^i\mathbf{r}_f\|^3} - n^2 & 0 & 0\\ 0 & \frac{\mu}{\|{}^i\mathbf{r}_f\|^3} - n^2 & 0\\ 0 & 0 & \frac{\mu}{\|{}^i\mathbf{r}_f\|^3}\end{bmatrix}, \quad \mathbf{E}_t = -\mu\begin{bmatrix}\frac{\|{}^i\mathbf{r}_l\|}{\|{}^i\mathbf{r}_f\|^3} - \frac{1}{\|{}^i\mathbf{r}_l\|^2}\\ 0\\ 0\end{bmatrix}, \tag{5}$$

with n as the orbital rate given by

$$n = \sqrt{\frac{\mu}{\|{}^i\mathbf{r}_l\|^3}} \tag{6}$$

and the relative control force defined as

$$\mathbf{F}_t = \frac{1}{m_f}\mathbf{f}_f \tag{7}$$

where $\mathbf{f}_f$ is the actuator forces of the follower in the $\mathcal{F}^{lo}$ frame.

2.3 Relative Rotational Motion

Consider the unit quaternion $\mathbf{q}_s = \begin{bmatrix}\eta_s & \boldsymbol{\varepsilon}_s^T\end{bmatrix}^T \in \mathbb{H}$, $\eta_s \in \mathbb{R}$, $\boldsymbol{\varepsilon}_s \in \mathbb{R}^3$, with $\|\mathbf{q}_s\| = 1$, as the spacecraft attitude representation of the frame $\mathcal{F}^{sb}$ relative to $\mathcal{F}^{lo}$, $\mathbf{q}_f$ for the follower, $\mathbf{q}_l$ for the leader and $\mathbb{H}$ the set of all quaternions. Then, the relative quaternion between the leader and the follower is given by

$$\mathbf{q} = \mathbf{q}_f \otimes \bar{\mathbf{q}}_l = \begin{bmatrix}\eta_f\eta_l + \boldsymbol{\varepsilon}_f^T\boldsymbol{\varepsilon}_l\\ \eta_l\boldsymbol{\varepsilon}_f - \eta_f\boldsymbol{\varepsilon}_l - \mathbf{S}(\boldsymbol{\varepsilon}_f)\boldsymbol{\varepsilon}_l\end{bmatrix} = \begin{bmatrix}\eta\\ \boldsymbol{\varepsilon}\end{bmatrix} \tag{8}$$

where $\bar{\mathbf{q}} = \begin{bmatrix}\eta_s & -\boldsymbol{\varepsilon}_s^T\end{bmatrix}^T$ is the quaternion conjugate, $\mathbf{S}(.) \in \mathbb{R}^{3\times3}$ is the skew-symmetric matrix given by

$$\mathbf{S}(\boldsymbol{\varepsilon}) = \begin{bmatrix}0 & -\varepsilon_z & \varepsilon_y\\ \varepsilon_z & 0 & -\varepsilon_x\\ -\varepsilon_y & \varepsilon_x & 0\end{bmatrix}. \tag{9}$$

Thus, the relative attitude kinematics is [28]

$$\dot{\mathbf{q}} = \begin{bmatrix}\dot{\eta}\\ \dot{\boldsymbol{\varepsilon}}\end{bmatrix} = \frac{1}{2}\begin{bmatrix}-\boldsymbol{\varepsilon}^T\\ \eta\mathbf{I}_3 + \mathbf{S}(\boldsymbol{\varepsilon})\end{bmatrix}\boldsymbol{\omega} = \mathbf{T}\boldsymbol{\omega} \tag{10}$$

with $\boldsymbol{\omega} = \boldsymbol{\omega}_{lb,fb}^{fb} \in \mathbb{R}^3$ as the relative angular velocity, or the angular velocity of $\mathcal{F}^{fb}$ relative to $\mathcal{F}^{lb}$, expressed in the $\mathcal{F}^{fb}$ frame.

Considering the spacecraft as rigid bodies, the rotational dynamics can the expressed by Euler's equations of motion for a rigid body, given by

$$\mathbf{J}_s\dot{\boldsymbol{\omega}}_{i,sb}^{sb} = -\mathbf{S}(\boldsymbol{\omega}_{i,sb}^{sb})\mathbf{J}_s\boldsymbol{\omega}_{i,sb}^{sb} + \boldsymbol{\tau}_{sb} \tag{11}$$

where $\mathbf{J}_s \in \mathbb{R}^{3\times3}$ is the spacecraft moment of inertia matrix, $\boldsymbol{\omega}_{i,sb}^{sb}$ is the angular velocity of $\mathcal{F}^{sb}$ relative to $\mathcal{F}^{i}$, expressed in the $\mathcal{F}^{sb}$ frame, and $\boldsymbol{\tau}_{sb} \in \mathbb{R}^3$ is the spacecraft actuator torque expressed in the $\mathcal{F}^{sb}$ frame. Therefore, considering that the relative angular velocity is given by

$$\boldsymbol{\omega} = \boldsymbol{\omega}_{i,fb}^{fb} - \mathbf{R}_{lb}^{fb}\boldsymbol{\omega}_{i,lb}^{lb} \tag{12}$$

the relative attitude dynamics, also detailed in [27], can be expressed as

$$\mathbf{J}_f\dot{\boldsymbol{\omega}} = \mathbf{C}_r\boldsymbol{\omega} + \mathbf{E}_r + \mathbf{T}_r \tag{13}$$

where

$$\mathbf{C}_r = -\mathbf{J}_f\mathbf{S}(\mathbf{R}_{lb}^{fb}\boldsymbol{\omega}_{i,lb}^{lb}) - \mathbf{S}(\mathbf{R}_{lb}^{fb}\boldsymbol{\omega}_{i,lb}^{lb})\mathbf{J}_f + \mathbf{S}(\mathbf{J}_f(\boldsymbol{\omega} + \mathbf{R}_{lb}^{fb}\boldsymbol{\omega}_{i,lb}^{lb})) \tag{14}$$

is a skew-symmetric matrix,

$$\mathbf{E}_r = -\mathbf{S}(\mathbf{R}_{lb}^{fb}\boldsymbol{\omega}_{i,lb}^{lb})\mathbf{J}_f\mathbf{R}_{lb}^{fb}\boldsymbol{\omega}_{i,lb}^{lb} + \mathbf{J}_f\mathbf{R}_{lb}^{fb}\mathbf{J}_l^{-1}\mathbf{S}(\boldsymbol{\omega}_{i,lb}^{lb})\mathbf{J}_l\boldsymbol{\omega}_{i,lb}^{lb}, \tag{15}$$

$$\mathbf{T}_r = \boldsymbol{\tau}_{fb} - \mathbf{J}_f\mathbf{R}_{lb}^{fb}\mathbf{J}_l^{-1}\boldsymbol{\tau}_{lb} \tag{16}$$

is the relative actuator torque and $\mathbf{R}_{lb}^{fb} \in \mathcal{SO}(3)$ is the rotation matrix from the leader body frame $\mathcal{F}^{lb}$ to the follower body frame $\mathcal{F}^{fb}$, defined using the relative quaternion $\mathbf{q}$ as

$$\mathbf{R}_{lb}^{fb} = \mathbf{I}_3 + 2\eta\mathbf{S}(\boldsymbol{\varepsilon}) + 2\mathbf{S}^2(\boldsymbol{\varepsilon}). \tag{17}$$

3 Distributed MPC for Spacecraft Platooning

Consider a system composed of λ spacecraft with masses m_i, $i = 1,2,...,\lambda$, such that, spacecraft $i \neq 1$ wants to follow spacecraft $i-1$ in a V-bar station keeping trajectory [29] and is followed by spacecraft $i+1$ the same way, being spacecraft $i = 1$ the leader of the platooning system. Furthermore, in this Section, the leader-follower topology is considered every time the whole system is referenced, while the target-chaser topology refers to a sub-system, composed of only 2 spacecraft.

3.1 Joint Model

Assuming that the target spacecraft is in a circular orbit about the Earth, and that the relative position between the spacecraft is much smaller compared with the distance to the centre of the Earth, with a maximum relative position into the tens of kilometers [30, 31], expression (4) can be linearized around the origin of $\mathcal{F}^{to}$ to get the well known Clohessy-Wiltshire (CW) equations [32], in a target-chaser formation.

One assumption of the CW equations is that the target stays passive, meaning that the target control force is zero. Conversely, in the proposed formulation the CW equations must be modified in order to get a coupled relative motion between every spacecraft, where the control action acts as the link between all the relative models.

Applying the Taylor series expansion to expression (4) around the origin of $\mathcal{F}^{to}$ [31, Appendix A] and adding the target control force yields

$$\begin{cases} \ddot{x} - 3n^2x - 2n\dot{y} = u_{c,x} - u_{t,x} \\ \ddot{y} + 2n\dot{x} = u_{c,y} - u_{t,y} \\ \ddot{z} + n^2z = u_{c,z} - u_{t,z} \end{cases} \tag{18}$$

where $\mathbf{u}_c = \frac{1}{m_c}\mathbf{f}_c = \begin{bmatrix} u_{c,x} & u_{c,y} & u_{c,z} \end{bmatrix}^T$ is the control force from the chaser and $\mathbf{u}_t = \frac{1}{m_t}\mathbf{f}_t = \begin{bmatrix} u_{t,x} & u_{t,y} & u_{t,z} \end{bmatrix}^T$ is the control force from the target. Then, with expression (18) and knowing that $\mathbf{v} = \dot{\mathbf{p}}$, the linear state-space model in a target-chaser formation is given by

$$\dot{\mathbf{x}}_{tc}(t) = \mathbf{A}'\mathbf{x}_{tc}(t) + \mathbf{B}'\mathbf{u}_c(t) - \mathbf{B}'\mathbf{u}_t(t) \tag{19}$$

where $\mathbf{x}_{tc} = \begin{bmatrix} \mathbf{p}_{tc}^T & \mathbf{v}_{tc}^T \end{bmatrix}^T = \begin{bmatrix} x_{tc} & y_{tc} & z_{tc} & \dot{x}_{tc} & \dot{y}_{tc} & \dot{z}_{tc} \end{bmatrix}^T$ is the state vector,

$$\mathbf{A}' = \begin{bmatrix} 0 & 0 & 0 & 1 & 0 & 0 \\ 0 & 0 & 0 & 0 & 1 & 0 \\ 0 & 0 & 0 & 0 & 0 & 1 \\ 3n^2 & 0 & 0 & 0 & 2n & 0 \\ 0 & 0 & 0 & -2n & 0 & 0 \\ 0 & 0 & -n^2 & 0 & 0 & 0 \end{bmatrix}, \quad \mathbf{B}' = \begin{bmatrix} 0 & 0 & 0 \\ 0 & 0 & 0 \\ 0 & 0 & 0 \\ 1 & 0 & 0 \\ 0 & 1 & 0 \\ 0 & 0 & 1 \end{bmatrix} \tag{20}$$

with n as the orbital rate of the leader.

Finally, the joint relative model is given by

$$\begin{bmatrix} \dot{\mathbf{x}}_{12}(t) \\ \dot{\mathbf{x}}_{23}(t) \\ \vdots \\ \dot{\mathbf{x}}_{\lambda-1,\lambda}(t) \end{bmatrix} = \begin{bmatrix} \mathbf{A}' & 0 & \cdots & 0 \\ 0 & \mathbf{A}' & \cdots & 0 \\ \vdots & \vdots & \ddots & \vdots \\ 0 & 0 & \cdots & \mathbf{A}' \end{bmatrix} \begin{bmatrix} \mathbf{x}_{12}(t) \\ \mathbf{x}_{23}(t) \\ \vdots \\ \mathbf{x}_{\lambda-1,\lambda}(t) \end{bmatrix} + \begin{bmatrix} -\mathbf{B}' & \mathbf{B}' & 0 & \cdots & 0 \\ 0 & -\mathbf{B}' & \mathbf{B}' & \cdots & 0 \\ \vdots & \vdots & \vdots & \ddots & \vdots \\ 0 & 0 & 0 & \cdots & \mathbf{B}' \end{bmatrix} \begin{bmatrix} \mathbf{u}_1(t) \\ \mathbf{u}_2(t) \\ \mathbf{u}_3(t) \\ \vdots \\ \mathbf{u}_\lambda(t) \end{bmatrix} \tag{21}$$

for which a Zero-Order Hold (ZOH) discretization is performed, as suggested in [33], in order to work with the following discrete MPC design, with the position as the system output.

3.2 Distributed Model Predictive Control (DMPC)

Consider a time-invariant linear discrete-time system with sampling time T_s, state $\mathbf{x} \in \mathbb{R}^a$, input $\mathbf{u} \in \mathbb{R}^b$ and output $\mathbf{y} \in \mathbb{R}^c$ described by

$$\mathbf{x}^+ = \mathbf{A}\mathbf{x} + \mathbf{B}\mathbf{u} \tag{22}$$

$$\mathbf{y} = \mathbf{C}\mathbf{x} \tag{23}$$

that represents a joint coupled model with M agents, such that,

$$\mathbf{x} = \begin{bmatrix} \mathbf{x}_1 \\ \vdots \\ \mathbf{x}_M \end{bmatrix}, \mathbf{u} = \begin{bmatrix} \mathbf{u}_1 \\ \vdots \\ \mathbf{u}_M \end{bmatrix}, \mathbf{U} = \begin{bmatrix} \mathbf{u}(0) \\ \vdots \\ \mathbf{u}(N-1) \end{bmatrix}, \mathbf{A} = \begin{bmatrix} \mathbf{A}_1 & \cdots & 0 \\ \vdots & \ddots & \vdots \\ 0 & \cdots & \mathbf{A}_M \end{bmatrix}, \quad \mathbf{B} = \begin{bmatrix} \mathbf{B}_1 \\ \vdots \\ \mathbf{B}_M \end{bmatrix}. \tag{24}$$

Consider also that these agents share a common objective, given by the cooperative cost

$$\mathbf{V}(\mathbf{x}(0), \mathbf{U}) = \sum_{j=1}^{M} \alpha_j \mathbf{V}_j(\mathbf{x}_j(0), \mathbf{U}) \tag{25}$$

where for each agent j, the cooperative quadratic tracking cost is

$$\mathbf{V}(\mathbf{x}(0),\mathbf{U}) = \mathbf{l}_j(\mathbf{y}(N)-\mathbf{y}_d(N)) + \sum_{k=0}^{N-1} \mathbf{s}_j(\mathbf{y}(k)-\mathbf{y}_d(k),\mathbf{u}(k)) \tag{26}$$

with

$$\mathbf{s}_j(\mathbf{y}_e,\mathbf{u}) = \mathbf{y}_e^T \operatorname{diag}(\alpha_1\mathbf{Q}_1,\cdots,\alpha_M\mathbf{Q}_M)\mathbf{y}_e + \mathbf{u}_j^T\,\alpha_j\mathbf{H}_j\mathbf{u}_j + \text{cnst}, \tag{27}$$

$$\mathbf{l}_j(\mathbf{y}_e) = \mathbf{y}_e^T \operatorname{diag}(\alpha_1\mathbf{P}_1,\cdots,\alpha_M\mathbf{P}_M)\mathbf{y}_e \tag{28}$$

and where N is the prediction horizon, $\mathbf{y}_d \in \mathbb{R}^c$ is the desired output, α is the relative weight in the overall objective, $\mathbf{P}$ is the final output error penalty, $\mathbf{Q}$ is the output error penalty and $\mathbf{H}$ is the control action penalty.

Then, the constrained optimal control problem for each agent is defined as

$$\begin{aligned} \min_{\mathbf{U}_j} \quad & \mathbf{V}(\mathbf{x}(0),\mathbf{U}) \\ \text{s.t.} \quad & \mathbf{x}^+ = \mathbf{A}\mathbf{x}+\mathbf{B}\mathbf{u}, \quad \mathbf{y} = \mathbf{C}\mathbf{x}, \quad \forall_{k=0,\ldots,N-1}, \\ & \mathbf{x} \in \mathcal{X}, \quad \mathbf{u}_j \in \mathcal{U}_j, \quad \forall_{k=0,\ldots,N-1}, \\ & \mathbf{x}(N) \in \mathcal{X}_f \end{aligned} \tag{29}$$

where $\mathcal{U}$ and $\mathcal{X}$ are the constraint sets on the control and state variables, respectively and k is the current time step.

To ensure the convergence of the distributed algorithm, a convex step procedure is added, where the next iterate $\mathbf{U}_j^{\gamma+1}$ is a convex combination of the the current optimal solution, $\mathbf{U}_j^*$, and the current iterate, $\mathbf{U}_j^\gamma$, given by [34]

$$\mathbf{U}_j^{\gamma+1} = w_j\mathbf{U}_j^* + (1-w_j)\mathbf{U}_j^\gamma, \quad 0 < w_j < 1 \tag{30}$$

where γ is the integer-valued iteration and w is the combination weight where $\sum_{j=1}^{M} w_j = 1$ and such that when expanding $\mathbf{U}_j^*$ and $\mathbf{U}_j^\gamma$ we have the contribution of the other agents. Although more realistic distributed algorithms can be considered that take into account different network topologies, this is left as future work.

3.3 Constraints

One of the more common and useful constraints is the control action constraint, in order to limit the energy consumed by the thrusters, given by $\mathbf{u}_{min} < \mathbf{u} < \mathbf{u}_{max}$. Relative velocity constraints are also important for spacecraft proximity operations, in order to better react to emergencies, unforeseen scenarios that may happen or to prepare for docking, $\mathbf{v}_{min} < \mathbf{v} < \mathbf{v}_{max}$.

Since this system consists of several spacecraft following each other, collision avoidance constraints are fundamental in order to avoid the collision between the spacecraft or to avoid space debris in the neighborhood. Mathematically, a collision avoidance constraint can be defined as

$$(x-x_\delta)^2 + (y-y_\delta)^2 + (z-z_\delta)^2 \geq r_\delta^2 \tag{31}$$

where $\mathbf{p}_\delta = \begin{bmatrix} x_\delta & y_\delta & z_\delta \end{bmatrix}^T$ is the position of the obstacle in the $\mathcal{F}^{to}$ frame, and r_δ is the minimum distance between the chaser and the debris.

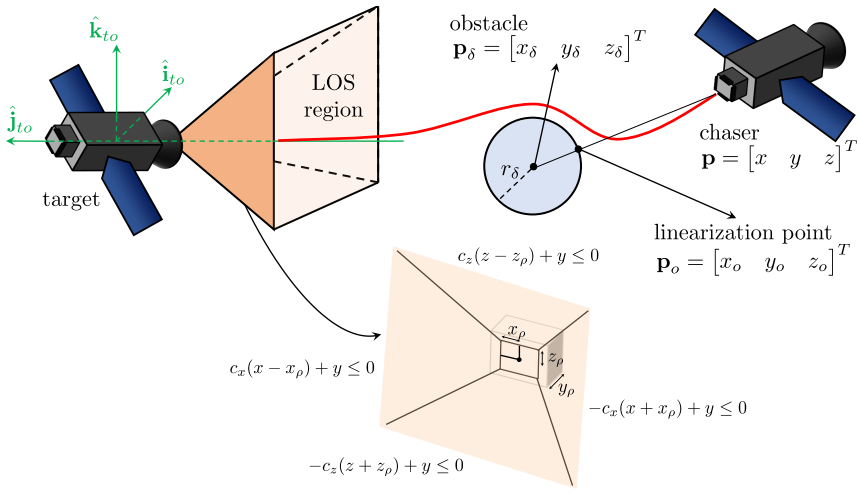

Fig. 2 LOS and collision avoidance constraint representation

Considering the object to avoid as a sphere, expression (31) can be linearized around the point located at $\mathbf{p}_o = \begin{bmatrix} x_o & y_o & z_o \end{bmatrix}^T$, determined by the intersection between the sphere surface and the imaginary line that goes from the center of the sphere to the chaser, which is reasonable for the considered scales. Applying the Taylor series expansion, the collision avoidance can be rewritten as $\mathbf{a}_{obs}\mathbf{x} \leq \mathbf{b}_{obs}$ [35] with

$$\mathbf{a}_{obs} = -2\begin{bmatrix} x_o - x_\delta & y_o - y_\delta & z_o - z_\delta & 0 & 0 & 0 \end{bmatrix}, \tag{32}$$

$$\mathbf{b}_{obs} = (x_o - x_\delta)^2 + (y_o - y_\delta)^2 + (z_o - z_\delta)^2 - 2(x_o - x_\delta)x_o - 2(y_o - y_\delta)y_o - 2(z_o - z_\delta)z_o - r_\delta^2. \tag{33}$$

Path constraints must be also employed, to make sure the chaser spacecraft is visible all the time from the target port dock. For that, a Line-Of-Sight (LOS) region is defined around the target port and expressed in the $\mathcal{F}^{to}$ frame, which yields [36]

$$\mathbf{a}_{los}\mathbf{x} \leq \mathbf{b}_{los} \Leftrightarrow \begin{bmatrix} 0 & 1 & 0 & 0 & 0 & 0 \\ c_x & 1 & 0 & 0 & 0 & 0 \\ -c_x & 1 & 0 & 0 & 0 & 0 \\ 0 & 1 & c_z & 0 & 0 & 0 \\ 0 & 1 & -c_z & 0 & 0 & 0 \end{bmatrix} \mathbf{x} \leq \begin{bmatrix} -y_\rho \\ c_x x_\rho \\ c_x x_\rho \\ c_z z_\rho \\ c_z z_\rho \end{bmatrix} \tag{34}$$

where c_x and c_z are the slopes of the tetrahedral cone, and $\begin{bmatrix} x_\rho & y_\rho & z_\rho \end{bmatrix}$ are the target port dimensions, as can be seen by the Fig. 2 along with the collision avoidance constraint. Simulation results for this system are presented in Section 5 to analyze the performance and validate the proposed strategy.

4 Cooperative MPC for On-Orbit Spacecraft Servicing

Consider a system composed of λ spacecraft with masses m_i, $i = 1, 2, ..., \lambda$, such that, every spacecraft moves around a passive object that can be bounded by a spherical region of radius r_σ and acts as the origin of $\mathcal{F}^{lo}$, therefore, every spacecraft position can be determined by the relative position between each spacecraft and the passive object. In addition to that, consider that the $\mathcal{F}^{lo}$ frame coincides with the $\mathcal{F}^{lb}$ frame.

4.1 6DOF Model

Recalling the expression for the relative translation (4) and relative rotation (13), a 6DOF (6 Degrees of Freedom) model can be formulated for each spacecraft with the state vector $\mathbf{x} = \begin{bmatrix}\mathbf{p}^T & \mathbf{v}^T & \mathbf{q}^T & \boldsymbol{\omega}^T\end{bmatrix}^T$ which yields the following nonlinear model

$$\begin{cases}\dot{\mathbf{p}} = \mathbf{v}, \\ \dot{\mathbf{v}} = \mathbf{D}_t\mathbf{p} + \mathbf{C}_t\mathbf{v} + \mathbf{F}_{tf}\mathbf{u}_f + \mathbf{E}_t, \\ \dot{\mathbf{q}} = \mathbf{T}\boldsymbol{\omega}, \\ \dot{\boldsymbol{\omega}} = \mathbf{J}_f^{-1}\mathbf{C}_r\boldsymbol{\omega} + \mathbf{J}_f^{-1}\mathbf{F}_{rf}\mathbf{u}_f + \mathbf{J}_f^{-1}\mathbf{E}_r\end{cases} \tag{35}$$

where $\mathbf{F}_{tf}$ and $\mathbf{F}_{rf}$ are the thruster configuration matrices for the follower actuator forces and the follower actuator torques respectively, such that $\mathbf{F}_t = \mathbf{F}_{tf}\mathbf{u}_f, \quad \mathbf{T}_r = \mathbf{F}_{rf}\mathbf{u}_f$ [37] with

$$\mathbf{F}_{tf} = \begin{bmatrix}0 & 0 & 1 & -1 & 0 & 0 \\ 0 & 0 & 0 & 0 & 1 & -1 \\ 1 & -1 & 0 & 0 & 0 & 0\end{bmatrix}, \quad \mathbf{F}_{rf} = \begin{bmatrix}\frac{L_y}{2} & \frac{L_y}{2} & 0 & 0 & \frac{L_z}{2} & \frac{L_z}{2} \\ -\frac{L_x}{2} & -\frac{L_x}{2} & \frac{L_z}{2} & \frac{L_z}{2} & 0 & 0 \\ 0 & 0 & -\frac{L_y}{2} & -\frac{L_y}{2} & \frac{L_x}{2} & \frac{L_x}{2}\end{bmatrix} \tag{36}$$

being $\begin{bmatrix}L_x & L_y & L_z\end{bmatrix}$ the spacecraft dimensions, and $\mathbf{u}_f = \begin{bmatrix}u_{f1} & u_{f2} & u_{f3} & u_{f4} & u_{f5} & u_{f6}\end{bmatrix}^T$ as can be seen in [37].

4.2 Nonlinear Model Predictive Control (NMPC)

Consider a nonlinear discrete-time system with sampling time T_s, state $\mathbf{x}$, and input $\mathbf{u}$, described by the difference equation

$$\mathbf{x}^+ = \mathbf{g}(\mathbf{x}, \mathbf{u}) \tag{37}$$

that represents the discrete state-space relative model from expression (35), with a constrained optimal control problem defined as

$$\begin{aligned}\min_{\mathbf{U}} \quad & \mathbf{V}(\mathbf{x}(0), \mathbf{u}) \\ \text{s.t.} \quad & \mathbf{x}^+ = \mathbf{g}(\mathbf{x}, \mathbf{u}), \quad \forall_{k=0,\ldots,N-1}, \\ & \mathbf{x} \in \mathcal{X}, \quad \mathbf{u} \in \mathcal{U}, \quad \forall_{k=0,\ldots,N-1}.\end{aligned} \tag{38}$$

This optimal control problem is a nonlinear programming (NLP) optimization problem with the cost function

$$\begin{aligned}\mathbf{V}(\mathbf{x}(0), \mathbf{u}) = \sum_{k=0}^{N-1} & (\mathbf{p} - \mathbf{p}_d)^T\mathbf{Q}_p(\mathbf{p} - \mathbf{p}_d) + (\mathbf{v} - \mathbf{v}_d)^T\mathbf{Q}_v(\mathbf{v} - \mathbf{v}_d) + \\ + & \begin{bmatrix}1 - \tilde{\eta} \\ \tilde{\boldsymbol{\varepsilon}}\end{bmatrix}^T \mathbf{Q}_q \begin{bmatrix}1 - \tilde{\eta} \\ \tilde{\boldsymbol{\varepsilon}}\end{bmatrix} + (\boldsymbol{\omega} - \boldsymbol{\omega}_d)^T\mathbf{Q}_w(\boldsymbol{\omega} - \boldsymbol{\omega}_d) + \mathbf{u}^T\mathbf{H}\mathbf{u}\end{aligned} \tag{39}$$

where $\mathbf{p}_d$, $\mathbf{v}_d$ and $\boldsymbol{\omega}_d$ are respectively the desired position, velocity and angular velocity, $\tilde{\mathbf{q}} = \begin{bmatrix}\tilde{\eta} & \tilde{\boldsymbol{\varepsilon}}^T\end{bmatrix}^T$ is the quaternion error and $\mathbf{Q}_p \in \mathbb{R}^{3\times3}$, $\mathbf{Q}_v \in \mathbb{R}^{3\times3}$, $\mathbf{Q}_q \in \mathbb{R}^{4\times4}$ and $\mathbf{Q}_w \in \mathbb{R}^{3\times3}$ the position, velocity, quaternion and angular velocity penalties respectively.

4.3 Constraints

Regarding the constraints, some can be reused for this scenario, namely the control action constraint, the velocity constraint and the quadratic collision avoidance constraint expressed in sub Section 3.3. For the collision avoidance constraint there will be considered two different scenarios, first a constraint to avoid the object located at the origin of $\mathcal{F}^{lo}$, resulting in the constraint

$$x^2 + y^2 + z^2 \geq (r_\sigma + r_s)^2 \tag{40}$$

where r_σ is the spherical radius that bounds the object and r_s is the spacecraft maximum radius. In addition to that, a coupled collision avoidance constraint must be considered in order to prevent the collision between the spacecraft that are moving around the object, that can be defined as

$$(x_i - x_j)^2 + (y_i - y_j)^2 + (z_i - z_j)^2 \geq (r_i + r_j)^2 \tag{41}$$

where spacecraft $i \neq j$. Finally, a angular velocity constraint can be incorporated, defined as

$$\boldsymbol{\omega}_{min} < \boldsymbol{\omega} < \boldsymbol{\omega}_{max}. \tag{42}$$

4.4 Attitude Trajectory Planning

Consider a fixed point with position $\mathbf{t}$ in the $\mathcal{F}^{lo}$ frame, in such a way that the spacecraft changes its attitude in order to point directly to $\mathbf{t}$, resorting only to relative attitude dynamics. For that, a vector must be assigned, that goes from the spacecraft to $\mathbf{t}$ in the $\mathcal{F}^{fo}$ frame, which yields

$$\mathbf{t}^{fo} = \mathbf{R}_{lo}^{fo}(-\mathbf{p} + \mathbf{t}). \tag{43}$$

So, a desired reference frame $\mathcal{F}^d : \{O_f, \hat{\mathbf{i}}_d, \hat{\mathbf{j}}_d, \hat{\mathbf{k}}_d\}$ can be defined as

$$\hat{\mathbf{k}}_d = \mathbf{t}^{fo}/\|\mathbf{t}^{fo}\|, \quad \hat{\mathbf{j}}_d = \hat{\mathbf{k}}_d \times \mathbf{p}/\|\hat{\mathbf{k}}_d \times \mathbf{p}\|, \quad \hat{\mathbf{i}}_d = \hat{\mathbf{j}}_d \times \hat{\mathbf{k}}_d \tag{44}$$

in order to point to $\mathbf{t}$ but also to fix the spacecraft orientation, for mathematical convenience. Reference frame that allows to obtain the desired angular velocity [38]

$$\boldsymbol{\omega}_{fo,d}^{d} = \begin{bmatrix} -\frac{\dot{\mathbf{t}}^{fo} \cdot \hat{\mathbf{j}}_d}{\|\mathbf{t}^{fo}\|} & \frac{\dot{\mathbf{t}}^{fo} \cdot \hat{\mathbf{i}}_d}{\|\mathbf{t}^{fo}\|} & 0 \end{bmatrix}^T \tag{45}$$

where

$$\dot{\mathbf{t}}^{fo} = \mathbf{S}(\boldsymbol{\omega}_{fo,lo}^{fo})\mathbf{t}^{fo} + \mathbf{R}_{lo}^{fo}(-\dot{\mathbf{p}} + \dot{\mathbf{t}}) \tag{46}$$

but, considering that $\mathcal{F}^{lo}$ is parallel to $\mathcal{F}^{fo}$, since the distance between the spacecraft is much closer than the orbit radius, an approximation can be made, with $\boldsymbol{\omega}_{fo,lo}^{fo} \approx \mathbf{0}$ and $\mathbf{R}_{lo}^{fo} \approx \mathbf{I}_3$, such that

$$\dot{\mathbf{t}}^{fo} = -\dot{\mathbf{p}}. \tag{47}$$

The expression (45) allows to obtain the relative angular velocity error defined as

$$\tilde{\boldsymbol{\omega}} = \boldsymbol{\omega} - \boldsymbol{\omega}_d = \boldsymbol{\omega}_{lb,fb}^{fb} - \boldsymbol{\omega}_{lb,d}^{fb} \tag{48}$$

with

$$\boldsymbol{\omega}_d = \boldsymbol{\omega} - \boldsymbol{\omega}_{fo,fb}^{fb} + \mathbf{R}_d^{fb}\boldsymbol{\omega}_{fo,d}^{d} = -\mathbf{R}_{lb}^{fb}\boldsymbol{\omega}_{i,lb}^{lb} + \mathbf{R}_{fo}^{fb}(\boldsymbol{\omega}_{i,fo}^{fo} + \mathbf{R}_d^{fo}\boldsymbol{\omega}_{fo,d}^{d}) \tag{49}$$

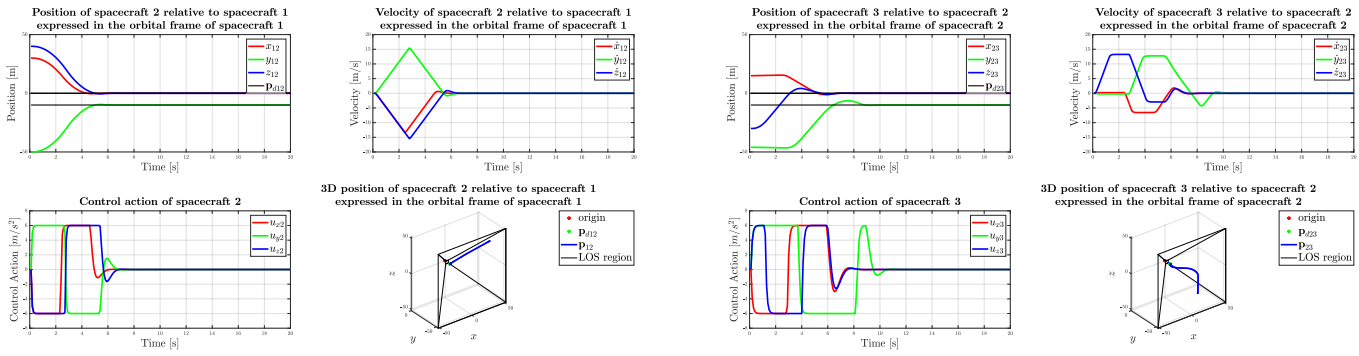

(a) Spacecraft 1 **(b) Spacecraft 2**

Fig. 3 DMPC spacecraft platooning simulation results

where $\boldsymbol{\omega}_{i,lb}^{lb} = \begin{bmatrix} 0 & 0 & n_l \end{bmatrix}^T$ and since it is assumed that $\mathcal{F}^{lo}$ coincides with $\mathcal{F}^{lb}$, $\mathbf{R}_{fo}^{fb}$ can be determined from $\mathbf{q}_f$. Also, $\boldsymbol{\omega}_{i,fo}^{fo} = \begin{bmatrix} 0 & 0 & n_f \end{bmatrix}^T$ and $\mathbf{R}_d^{fo}$ can be determined from the basis vectors of $\mathcal{F}^d$ (44). On the other hand, the quaternion error is defined as $\tilde{\mathbf{q}} = \mathbf{q}_f \otimes \bar{\mathbf{q}}_d$ where $\mathbf{q}_d$ can be obtained from $\mathbf{R}_{fo}^d$.

Simulation results for this system are presented in Section 5 to analyze the performance and validate the proposed strategy.

5 Simulation Results

This Section describes the simulation details and presents the results for both control strategies presented in Sections 3 and 4, followed by the discussion of these results. All simulations have been performed in MATLAB® R2019A, considering $T_s = 0.1$s and $\|{}^i\mathbf{r}_l\| = 6621$km.

5.1 Distributed MPC for Spacecraft Platooning

Consider a simulation scenario with $\mathbf{p}_{12}(0) = \begin{bmatrix} 30 & -50 & 40 \end{bmatrix}^T$ m, $\mathbf{p}_{23}(0) = \begin{bmatrix} 15 & -46 & -30 \end{bmatrix}^T$ m, $\mathbf{v}_{tc}(0) = \mathbf{0}_{3\times1}\mathrm{m\,s^{-1}}$, $\mathbf{y}_d = \begin{bmatrix} 0 & -10 & 0 \end{bmatrix}^T$ m, $\mathbf{P} = 25I_3$, $\mathbf{Q} = 8I_3$, $\mathbf{H} = 0.1I_3$, $\mathbf{p}_\delta = \mathbf{0}_{3\times1}$m, $\begin{bmatrix} \alpha_1 & \alpha_2 \end{bmatrix} = \begin{bmatrix} 2 & 1.5 \end{bmatrix}$, $\begin{bmatrix} c_x & c_z \end{bmatrix} = \begin{bmatrix} 1 & 1 \end{bmatrix}$, $\begin{bmatrix} x_\rho & y_\rho & z_\rho \end{bmatrix} = \begin{bmatrix} 2 & 2 & 4 \end{bmatrix}$ m, $\begin{bmatrix} w_1 & w_2 \end{bmatrix} = \begin{bmatrix} 0.6 & 0.4 \end{bmatrix}$, $r_\delta = 6$m, $\gamma = 2$, $u_{max} = 6\mathrm{m\,s^{-2}}$, $v_{max} = 20\mathrm{m\,s^{-1}}$ and $N = 40$.

Given the parameters above, the simulation can be seen in Fig. 3, for a system composed by 3 spacecraft where the leader remains passive. From Fig. 3 it is showcased that each spacecraft is able to perform the approximation and maintain a constant V-Bar position between each other while satisfying all the constraints considered for this scenario at all times.

5.2 Cooperative MPC for On-Orbit Spacecraft Servicing

Consider a simulation scenario with simulation parameters given by $\mathbf{J}_f = \begin{bmatrix} 10 & 2.5 & 3.5 \\ 2.5 & 10 & 4.5 \\ 3.5 & 4.5 & 10 \end{bmatrix}$ kg m^2, $\mathbf{J}_l = \mathrm{diag}(10, 10, 10)$ kg m^2, $N = 30$, $\mathbf{H} = 2I_6$, $\mathbf{Q}_p = 10I_3$, $\mathbf{Q}_v = 0.5I_3$, $\mathbf{Q}_q = 15I_4$, $\mathbf{Q}_w = 0.5I_3$, $\begin{bmatrix} L_x & L_y & L_z \end{bmatrix} = \begin{bmatrix} 2 & 2 & 2 \end{bmatrix}$ m, $u_{max} = 3\mathrm{m\,s^{-2}}$, $v_{max} = 5\mathrm{m\,s^{-1}}$, $\omega_{max} = 0.7\mathrm{rad\,s^{-1}}$, $r_\sigma = 12$m and $r_s = 3$m, whereas the ini-

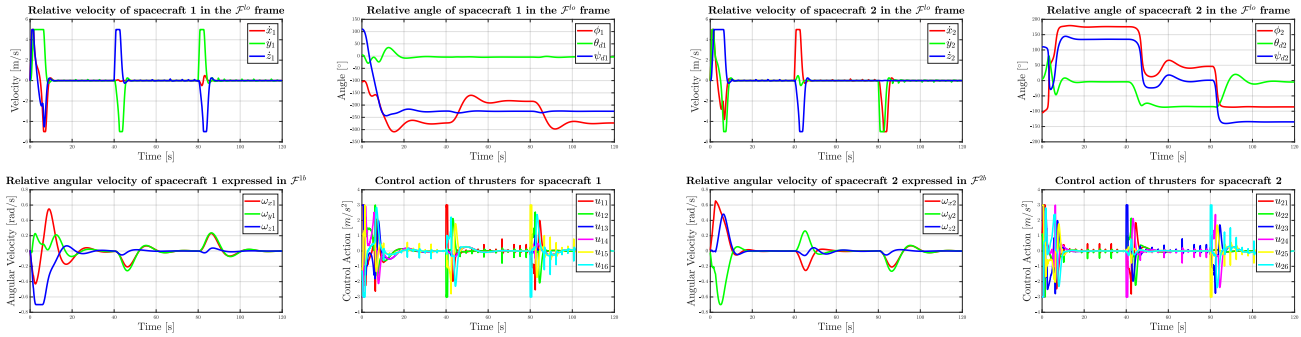

(a) Spacecraft 1 **(b) Spacecraft 2**

Fig. 4 NMPC on-orbit servicing simulation results: velocities, attitude and actuation

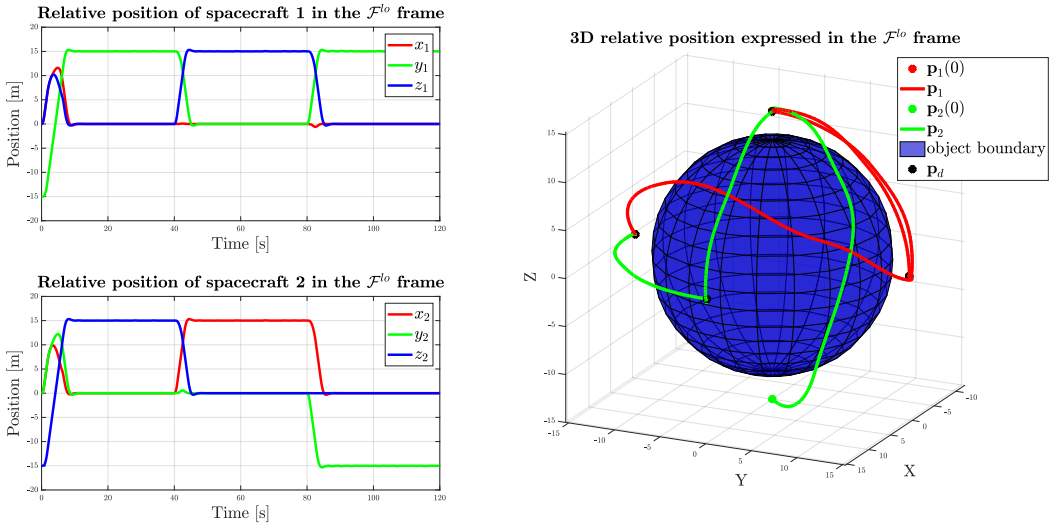

Fig. 5 NMPC on-orbit servicing simulation results: relative spacecraft positions

tial conditions are $\mathbf{p}_1(0) = \begin{bmatrix} 0 & -15 & 0 \end{bmatrix}^T$ m, $\mathbf{p}_2(0) = \begin{bmatrix} 0 & 0 & -15 \end{bmatrix}^T$ m, $\mathbf{q}(0) = \begin{bmatrix} 0.37 & -0.43 & 0.66 & 0.47 \end{bmatrix}^T$, $\mathbf{v}(0) = \mathbf{0}_{3\times 1}\,\mathrm{m\,s^{-1}}$, $\boldsymbol{\omega}(0) = \begin{bmatrix} 0.01 & -0.02 & 0.01 \end{bmatrix}^T\,\mathrm{rad\,s^{-1}}$, $\mathbf{v}_d = \mathbf{0}_{3\times 1}\,\mathrm{m\,s^{-1}}$, as also

$$\mathbf{p}_{d1} = \begin{cases} \begin{bmatrix} 0 & 15 & 0 \end{bmatrix}^T & \text{for } t \leq 40, \\ \begin{bmatrix} 0 & 0 & 15 \end{bmatrix}^T & \text{for } 40 < t \leq 80, \\ \begin{bmatrix} 0 & 15 & 0 \end{bmatrix}^T & \text{for } t > 80 \end{cases}, \quad \mathbf{p}_{d2} = \begin{cases} \begin{bmatrix} 0 & 0 & 15 \end{bmatrix}^T & \text{for } t \leq 40, \\ \begin{bmatrix} 15 & 0 & 0 \end{bmatrix}^T & \text{for } 40 < t \leq 80, \\ \begin{bmatrix} 0 & -15 & 0 \end{bmatrix}^T & \text{for } t > 80 \end{cases}. \tag{50}$$

The simulation results can be seen in Fig. 4 and 5, for a system composed by 2 spacecraft that point to a central object, resorting to the open-source tool for nonlinear optimization, CasADi [39]. For the simulation, consider also the Euler angles as the attitude representation, such that the quaternion results are converted to Euler angles through XYZ rotation. From Fig. 4 and 5 it is showcased not only that each spacecraft is able to follow the re-planned flight trajectory but at the same time point to the desired attitude while satisfying all the constraints considered in this scenario. It is necessary also to take into account the circular path that is carried out for each spacecraft in order to get around the central object, which results in a substantial overshoot for the relative position, but from Fig. 5 a smooth trajectory

can be seen around the object such as the collision constraint between the spacecraft and the object, constraint that is always satisfied.

6 Conclusion

The goal of this paper was to design and rethink the rendezvous problem, in a more cooperative and optimal solution for two different scenarios, spacecraft synchronization and on-orbit spacecraft servicing. For spacecraft synchronization, it was considered a distributed platooning system where an optimization problem was formulated with collision avoidance, LOS, and physical limitations constraints in order to generate better and safer trajectories. On the other hand, for on-orbit spacecraft servicing, a nonlinear optimization problem was formulated with two different collision avoidance constraints and capable of changing its attitude in order to point directly to the object. In a second stage, both systems were validated through simulated tests in MATLAB®, where different maneuvers are efficiently performed while satisfying all the constraints considered.

In terms of future work, there are some work directions that can be pursued. For the spacecraft platooning system, a network topology can be added and other distributed algorithms can be explored, together with more complex constraints and disturbances. For the on-orbit spacecraft servicing system, more advanced trajectory planning strategies can be incorporated, including a distributed network topology.

Acknowledgments

This work was partially funded by FCT project REPLACE (PTDC/EEIAUT/32107/2017) which includes Lisboa 2020 and PIDDAC funds, project CAPTURE (PTDC/EEIAUT/1732/2020), and also projects CTS (UIDB/00066/2020) and LARSYS (UIDB/50009/2020).

References

[1] D. C. Woffinden and D. K. Geller. Navigating the road to autonomous orbital rendezvous. *Journal Spacecraft Rockets*, 44(4), 2007. DOI: 10.2514/1.30734.

[2] Q. Li, J. Yuan, B. Zhang, and C. Gao. Model predictive control for autonomous rendezvous and docking with a tumbling target. In *Aerospace Science and Technology*, page 700–711, 2017. DOI: 10.1016/j.ast.2017.07.022.

[3] S. Kawamoto, T. Makida, F. Sasaki, Y. Okawa, and S. Nishida. Precise numerical simulations of electrodynamic tethers for an active debris removal system. *Acta Astronautica*, 59(1), 2006. DOI: 10.1016/j.actaastro.2006.02.035.

[4] S. Nishida, S. Kawamoto, Y. Okawa, F. Terui, and S. Kitamura. Space debris removal system using a small satellite. *Acta Astronautica*, 65(1), 2009. DOI: 10.1016/j.actaastro.2009.01.041.

[5] J. C. Liou, N. L. Johnson, and N. M. Hill. Controlling the growth of future leo debris populations with active debris removal. *Acta Astronautica*, 66(5), 2010. DOI: 10.1016/j.actaastro.2009.08.005.

[6] Vincent L. Pisacane and Robert C. Moore. *Fundamentals of Space Systems*. Oxford University Press, New York, USA, 1994.

[7] James R. Wertz and Wiley J. Larson. *Space Mission Analysis and Design*. Microcosm Press, Torrance, USA, 1999.

[8] J. B. Rawlings and D. Q. Mayne. *Model predictive control: theory and design*. Madison, Wisconsin: Nob Hill Publishing, 2015.

[9] M. Saponara et al. Model predictive control application to spacecraft rendezvous in mars sample return scenario. In *Progress in Flight Dynamics, Guidance, Navigation, Control, Fault Detection and Avionics*, page 137–158, 2013. DOI: 10.1051/eucass/201306137.

[10] A. Weiss, I. Kolmanovsky, M. Baldwin, and R. S. Erwin. Model predictive control of three dimensional spacecraft relative motion. In *2012 American Control Conference (ACC)*, page 173–178, 2012. DOI: 10.1109/ACC.2012.6314862.

[11] H. Park, S. Di Cairano, and I. Kolmanovsky. Model predictive control for spacecraft rendezvous and docking with a rotating/tumbling platform and for debris avoidance. In *Proceedings of the 2011 American Control Conference*, page 1922–1927, 2011. DOI: 10.1109/ACC.2011.5991151.

[12] P. A. Felisiak, K. Sibilski, W. Wroblewski, and J. Z. Sasiadek. Spacecraft rendezvous in elliptical orbit using nonlinear model predictive control. In *AIAA Guidance, Navigation and Control Conference*, 2014. DOI: 10.2514/6.2014-0090.

[13] A. Weiss, M. Baldwin, R. S. Erwin, and I. Kolmanovsky. Model predictive control for spacecraft rendezvous and docking: Strategies for handling constraints and case studies. *IEEE Transactions on Control Systems Technology*, 23(4), 2015. DOI: 10.1109/TCST.2014.2379639.

[14] E. N. Hartley, P. A. Trodden, A. G. Richards, and J. M. Maciejowski. Model predictive control system design and implementation for spacecraft rendezvous. *Control Engineering Practice*, 20(7), 2012. DOI: 10.1016/j.conengprac.2012.03.009.

[15] A. Richards and J. P. How. Model predictive control of vehicle maneuvers with guaranteed completion time and robust feasibility. In *Proceedings of the 2003 American Control Conference*, 2003. DOI: 10.1109/ACC.2003.1240467.

[16] H. Park, S. DiCairano, and I. Kolmanovsky. Model predictive control of spacecraft docking with a non-rotating platform. *IFAC Proceedings Volumes*, 44(1), 2011. DOI: 10.3182/20110828-6-IT-1002.00031.

[17] R. Vazquez, F. Gavilan, and E. F. Camacho. Trajectory planning for spacecraft rendezvous with on/off thrusters. *IFAC Proceedings Volumes*, 44(1), 2011. DOI: 10.3182/20110828-6-IT-1002.02445.

[18] S. Di Cairano, H. Park, and I. Kolmanovsky. Model predictive control approach for guidance of spacecraft rendezvous and proximity maneuvering. *International Journal of Robust and Nonlinear Control*, 22(12), 2012. DOI: 10.1002/rnc.2827.

[19] V. Manikonda, P. O. Arambel, M. Gopinathan, R. K. Mehra, and F. Y. Hadaegh. A model predictive control-based approach for spacecraft formation keeping and attitude control. In *Proceedings of the American Control Conference*, 1999. DOI: 10.1109/ACC.1999.786367.

[20] J. Scharnagl, P. Kremmydas, and K. Schilling. Model predictive control for continuous low thrust satellite formation flying. *IFAC-PapersOnLine*, 51, 2018. DOI: 10.1016/j.ifacol.2018.07.081.

[21] L. Breger and J. How. J2-modified gve-based mpc for formation flying spacecraft. In *AIAA Guidance, Navigation and Control Conference and Exhibit*, 2005. DOI: 10.2514/6.2005-5833.

[22] L. Breger. Model predictive control for formation flying spacecraft. Master's thesis, Dept. of Aeronautics and Astronautics, Massachusetts Institute of Technology, Massachusetts, USA, 2004.

[23] J. Scharnagl, F. Kempf, and K. Schilling. Combining distributed consensus with robust h∞-control for satellite formation flying. *Electronics*, 8(319), 2019. DOI: 10.3390/electronics8030319.

[24] N. R. Esfahani and K. Khorasani. A distributed model predictive control (mpc) fault reconfiguration strategy for formation flying satellites. *International Journal of Control*, 89(5), 2016. DOI: 10.1080/00207179.2015.1110753.

[25] D. Catanoso. Networked model predictive control for satellite formation flying. Master's thesis, Space Technology, Luleå University of Technology, Sweden, 2019.

[26] Y. Zheng, S. E. Li, K. Li, F. Borrelli, and J. K. Hedrick. Distributed model predictive control for heterogeneous vehicle platoons under unidirectional topologies. *IEEE Transactions on Control Systems Technology*, 25(3), 2017. DOI: 10.1109/TCST.2016.2594588.

[27] R. Kristiansen, E. Grøtli, P. Nicklasson, and J. Gravdahl. A model of relative translation and rotation in leader-follower spacecraft formations. *Modeling, Identification and Control (MIC)*, 28(1), 2007. DOI: 10.4173/mic.2007.1.1.

[28] O. Fjellstad. *Control of unmanned underwater vehicles in six degrees of freedom: A quaternion feedback approach*. PhD thesis, Dep. of Engineering Cybernetics, Norwegian University of Science and Technology, Trondheim, Norway, October 1994.

[29] Nicholas G. Ortolano. *Autonomous trajectory planning for satellite RPO and safety of flight using convex optimization*. PhD thesis, Aerospace Engineering, Utah State University, Utah, USA, 2018.

[30] C. Jewison. *Guidance and control for multi-stage rendezvous and docking operations in the presence of uncertainty*. PhD thesis, Dept. of Aeronautics and Astronautics, Massachusetts Institute of Technology, Massachusetts, USA, 2017.

[31] W. Fehse. *Automated Rendezvous and Docking of Spacecraft*. Cambridge University Press, Cambridge, UK, first edition, 2003.

[32] W. Clohessy and R. Wiltshire. Terminal guidance system for satellite rendezvous. *Journal of Aerospace Sciences*, 27(9), 1960. DOI: 10.2514/8.8704.

[33] Edward N. Hartley. A tutorial on model predictive control for spacecraft rendezvous. In *2015 European Control Conference (ECC)*, pages 1355–1361, 2015. DOI: 10.1109/ECC.2015.7330727.

[34] J. Rawlings, D. Mayne, and M. Diehl. *Model predictive control: Theory, computation and design*. Nob Hill Publishing, LLC, California, USA, second edition, 2019.

[35] L. Ravikumar, N. Philip, R. Padhi, and M. Bhat. Autonomous terminal maneuver of spacecrafts for rendezvous using model predictive control. In *2016 Indian Control Conference (ICC)*, 2016. DOI: 10.1109/INDIANCC.2016.7441108.

[36] O. B. Iskender, K. V. Ling, and V. Dubanchet. Constraints tightening approach towards model predictive control based rendezvous and docking with uncooperative targets. In *2018 European Control Conference (ECC)*, 2018. DOI: 10.23919/ECC.2018.8550224.

[37] Y. Yang. *Spacecraft modeling, attitude determination and control quaternion-based approach*. CRC Press, Maryland, USA, second edition, 2019.

[38] R. Schlanbusch, R. Kristiansen, and P. Nicklasson. Attitude reference generation for leader-follower formation with nadir pointing leader. In *Proceedings of the 2010 American Control Conference*, 2010. DOI: 10.1109/ACC.2010.5531599.

[39] Joel A E Andersson, Joris Gillis, Greg Horn, James B Rawlings, and Moritz Diehl. CasADi – A software framework for nonlinear optimization and optimal control. *Mathematical Programming Computation*, 11(1):1–36, 2019. DOI: 10.1007/s12532-018-0139-4.